

# Supplementary Material for “Exotic Non-Abelian Topological Defects in Lattice Fractional Quantum Hall States”

Zhao Liu,<sup>1</sup> Gunnar Möller,<sup>2,3</sup> and Emil J. Bergholtz<sup>4</sup>

<sup>1</sup>*Dahlem Center for Complex Quantum Systems and Institut für Theoretische Physik,  
Freie Universität Berlin, Arnimallee 14, 14195 Berlin, Germany*

<sup>2</sup>*Functional Materials Group, School of Physical Sciences, University of Kent, Kent CT2 7NZ, United Kingdom*

<sup>3</sup>*TCM Group, Cavendish Laboratory, University of Cambridge, Cambridge CB3 0HE, United Kingdom*

<sup>4</sup>*Department of Physics, Stockholm University, AlbaNova University Center, 106 91 Stockholm, Sweden*

**Short-range tight-binding Hamiltonian.** In the main text, we use a tight-binding Hamiltonian with local but long-range hopping for theoretical elegance. Now we show that we can obtain similar results with only short-range hopping.

First, we only keep the nearest-neighbor (NN) and next-nearest-neighbor (NNN) hopping in the tight-binding model, Eq. (1) in the main text. Thus, we obtain a new tight-binding model with short-range hopping

$$H'_0 = \sum_{j,k,\sigma} t'(z_j, z_k) a_{j, \mathcal{F}^{n_j k}(\sigma)}^\dagger a_{k,\sigma}, \quad (\text{S1})$$

where  $t'(z_j, z_k) = (-1)^{x+y+xy} e^{-\frac{\pi}{2}(1-\phi)|z|^2} e^{-i\pi\phi(x_j+x_k)y}$  for  $|z|^2 \leq 2$  and  $t'(z_j, z_k) = 0$  for  $|z|^2 > 2$ . The meanings of the symbols are the same as those in the main text.

Although the exact flatness of the lowest  $2\phi L_x L_y$  eigenstates in the absence of defects is lost due to the hopping truncation, we still find that defects have almost the same effect on the band structure of  $H'_0$  as that on  $H_0$  shown in the main text [Figs. S1 and S2]. The energies of some eigenstates localized near the defects deviate from the original bands, and the dispersion of the lowest  $2\phi L_x L_y + M$  eigenstates can be reduced by a local potential  $V = -\sum_{n=1}^{2\phi L_x L_y + M} \epsilon_n \mathcal{T}_R(|\psi_n\rangle\langle\psi_n|)$  with negligible influence on the pertinent eigenvector subspace of  $H'_0$ , where  $\epsilon_n$ 's and  $\psi_n$ 's are now the eigenvalues and eigenvectors of  $H'_0$  respectively. One can notice that such a flattening procedure works better for smaller  $\phi$ , as shown in Figs. S1 and S2.

We diagonalize the interaction projected onto the lowest  $2\phi L_x L_y + M$  eigenstates of  $H'_0$  to examine the topological degeneracy at various filling fractions. Strikingly, we can get the expected topological degeneracy even though we have truncated the hopping [Fig. S3].

Second, let us further truncate the hopping range to include *only the nearest-neighbor* terms of the conventional Harper-Hofstadter model [S1–S3], with the same type of defects added. Remarkably, the defect-enhanced eight-fold Laughlin degeneracy of projected interactions remains stable for small flux density  $\phi$  even in this case [Fig. S4]. These results imply that the long-range hopping is indeed not necessary for the realization of lattice genons, thus facilitating their experimental realization. A realization based on the nearest-neighbor Harper-Hofstadter model would provide an additional range of host states to explore, as single layers can be chosen to realize higher Chern number  $\mathcal{C}$  bands that support a series of

hierarchy states at filling factors  $\nu = r/(k\mathcal{C}r + 1)$ , with  $r \in \mathbb{Z}$  and  $k$  even (odd) for bosons (fermions) [S4].

**Simplified local potentials.** In the main text, we use an additional potential  $V = -\sum_{n=1}^{2\phi L_x L_y + M} \epsilon_n \mathcal{T}_R(|\psi_n\rangle\langle\psi_n|)$  that is localized near the ends of branch cuts in order to restore a flat lowest band. At  $R \rightarrow \infty$ , this flattening process by  $V$  is asymptotically exact in the sense that the lowest  $2\phi L_x L_y + M$  eigenstates of  $H_0 + V$  will become exactly degenerate again at zero energy and have the same eigenvectors as those of  $H_0$ . Although having an elegant mathematical form, the hopping range in  $V$  depends on  $R$ . In order to facilitate realistic experimental implementations, we now consider a simplified version of  $V$  that only contains single-site energies and NN hopping terms:  $\tilde{V} = \alpha \sum_{n=1}^{2M} \mathcal{T}_{R,\text{NN}}(|\psi_n\rangle\langle\psi_n|) + \beta \sum_{n=2\phi L_x L_y - M + 1}^{2\phi L_x L_y + M} \mathcal{T}_{R,\text{NN}}(|\psi_n\rangle\langle\psi_n|)$ . Here we only sum over the  $4M$  single-particle states with the largest deviations from the original band structure (see Sec. III in the main text).  $|\psi_n\rangle$ 's are still the eigenvectors of the tight-binding Hamiltonian before band corrections.  $\mathcal{T}_{R,\text{NN}}$  truncates  $|\psi_n\rangle\langle\psi_n|$  not only at the radius  $R$  around each defect, but also up to the NN hopping.  $\alpha$  and  $\beta$  are parameters which we need to optimize to pursue the flattest lowest band.

We find that  $\tilde{V}$  with small  $R$  is sufficient to flatten the lowest band, with negligible influence on the pertinent eigenvector subspace of the tight-binding Hamiltonian before band corrections. As shown in Fig. S5, a flat lowest band required by the RR state is restored by  $\tilde{V}$  for  $H_0$  [Eq. (1) in the main text] [Figs. S5(a) and (b)] as well as for the conventional Hofstadter model with defects at small flux density [Fig. S5(c)]. Therefore,  $\tilde{V}$ , which only contains single-site and NN terms near each defect, is potentially suitable for the experimental realization of genons. In practice, one can even simply it further by eliminating some terms with small coefficients from the simplified potential  $\tilde{V}$ .

**Straight branch cuts used in the main text.** For completeness, we indicate the precise positions of branch cuts used to generate the data in the main text. All cuts in the main text are oriented along the  $y$ -axis, and for such branch cuts connecting a pair of two defects with identical  $X_1$ -coordinate and positions  $(X_1, Y_1)$  and  $(X_1, Y_2)$  we use the more succinct notation  $(X_1, Y_1 \rightarrow Y_2)$ .

For  $\nu = 1/2$  with two pairs of defects (Fig. 3), two branch cuts are located at  $(0.5, 0.25 \rightarrow 1.75)$ ,  $(2.5, 0.25 \rightarrow 1.75)$  for  $L_x \times L_y = 4 \times 3$ ;  $(0.5, 0.5 \rightarrow 2.5)$ ,  $(2.5, 0.5 \rightarrow$

2.5) for  $L_x \times L_y = 4 \times 4$  and  $4 \times 5$ ;  $(0.25, 0.25 \rightarrow 1.75)$ ,  $(3.25, 0.25 \rightarrow 1.75)$  for  $L_x \times L_y = 6 \times 3$ ;  $(0.25, 0.5 \rightarrow 2.5)$ ,  $(3.25, 0.5 \rightarrow 2.5)$  for  $L_x \times L_y = 6 \times 4$ ; and  $(0.25, 0.75 \rightarrow 3.25)$ ,  $(3.25, 0.75 \rightarrow 3.25)$  for  $L_x \times L_y = 6 \times 5$ . For  $\nu = 1$  with one pair of defects [Fig. 4(a)], the branch cut is located at  $(0.5, 0.5 \rightarrow 2.5)$  for  $L_x \times L_y = 3 \times 4$ ;  $(0.5, 0.75 \rightarrow 3.25)$  for  $L_x \times L_y = 3 \times 5$ ; and  $(1.5, 0.25 \rightarrow 1.75)$  for  $L_x \times L_y = 4 \times 3$ . For  $\nu = 1$  with two pairs of defects [Fig. 4(b)], the branch cuts are located at  $(0.25, 0.5 \rightarrow 2.5)$ ,  $(1.75, 0.5 \rightarrow 2.5)$  for  $L_x \times L_y = 3 \times 4$  and  $(0.25, 0.75 \rightarrow 3.25)$ ,  $(1.75, 0.75 \rightarrow 3.25)$  for  $L_x \times L_y = 3 \times 5$ . For  $\nu = 3/2$  with one pair of defects [Fig. 4(e)], the branch cut is located at  $(0.25, 0.5 \rightarrow 2.5)$  for  $L_x \times L_y = 3 \times 4$ .

**Tilted branch cuts.** In the main text, we have presented data for branch cuts arranged in the  $y$ -direction, as detailed above. In addition, we now consider more general locations of defects that yield tilted branch cuts. In these general cases, we denote the branch cut connecting a pair of defects at  $(X_1, Y_1)$  and  $(X_2, Y_2)$  as  $(X_1, Y_1) \rightarrow (X_2, Y_2)$ . In the following we use the same tight-binding model  $H_0$  as in the main text.

With tilted branch cuts, we observe a similar effect of defects on the band structure as that in the main text [Fig. S6]. Moreover, the many-body spectra of projected interactions reproduce the expected topological degeneracy for the given number of branch cuts [Fig. S7].

#### Definition of particle entanglement spectra and state

**counting.** PES are a useful diagnostic for topological order. For a  $\mathcal{D}$ -fold degenerate ground-state manifold  $\{|\Psi_\alpha\rangle\}$  of  $N$  particles, we define the PES levels  $\xi$  as  $\xi \equiv -\ln \lambda$ , where the  $\lambda$ 's are the eigenvalues of the reduced density matrix  $\rho_A$  of  $N_A$  particles obtained by tracing out  $N_B = N - N_A$  particles from the whole system, i.e.,  $\rho_A = \text{Tr}_B \rho$  with  $\rho = \frac{1}{\mathcal{D}} \sum_{\alpha=1}^{\mathcal{D}} |\Psi_\alpha\rangle\langle\Psi_\alpha|$ . A gap in the PES is expected, below which the number of PES levels is the same as the counting of the corresponding quasihole excitation spectrum [S5], which in our case can be obtained from diagonalizing the interaction Hamiltonian of  $N_b^A$  particles on the same lattice size with the same branch cuts.

- 
- [S1] P. G. Harper, *Proc. Phys. Soc. A* **68**, 874 (1955)
  - [S2] M. Y. Azbel, *Energy Spectrum of a Conduction Electron in a Magnetic Field*, *Soviet Physics JETP* **19**, 634 (1964) [ZhETF, **46**, 929 (1964)].
  - [S3] D. Hofstadter, *Energy levels and wave functions of Bloch electrons in rational and irrational magnetic fields*, *Phys. Rev. B* **14**, 2239 (1976).
  - [S4] G. Möller, N. R. Cooper, *Fractional Chern Insulators in Harper-Hofstadter Bands with Higher Chern Number*, *Phys. Rev. Lett.* **115**, 126401 (2015).
  - [S5] N. Regnault and B. A. Bernevig, *Fractional Chern Insulator*, *Phys. Rev. X* **1**, 021014 (2011).

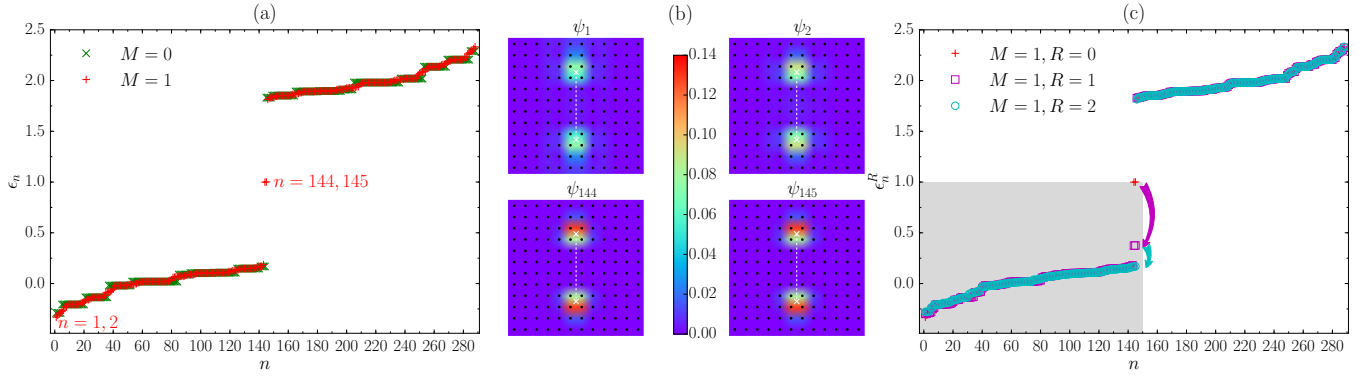


**Figure S1. Single-particle spectra and defect-induced localized states with NN and NNN hopping only.** We study the band structure on a  $L_x \times L_y = 12 \times 12$  lattice with  $\phi = 1/2$ . (a) The single-particle spectrum  $\{\epsilon_n\}$  of  $H'_0$ . In the absence of defects ( $M = 0$ ),  $\epsilon_1, \dots, \epsilon_{144}$  are no longer exactly degenerate at zero energy. With a branch cut ( $M = 1$ , white dashed line) at  $(5.5, 2.5 \rightarrow 8.5)$ , the original band structure is distorted, with one nearly degenerate cluster ( $\epsilon_{144}, \epsilon_{145}$ ) having the largest deviation. (b) The lattice site weight of eigenvectors  $\psi_1, \psi_2, \psi_{144}, \psi_{145}$  of  $H'_0$  for the same defects as in (a). All of them are strongly localized near the defects. However, the localization of  $\psi_1$  and  $\psi_2$  is weaker than the case of  $H_0$  in the main text, probably because now they have much less energy deviation from the original band structure. (c) The single-particle spectrum  $\{\epsilon_n^R\}$  of  $H'_0 + V$  with  $R = 0, 1$ , and  $2$  and the same defects as in (a). The degeneracy of  $\epsilon_1^R, \dots, \epsilon_{145}^R$  (shaded in gray) becomes better for larger  $R$ , with the flatness  $0.6, 2.2, 3.7$  for  $R = 0, 1, 2$ .

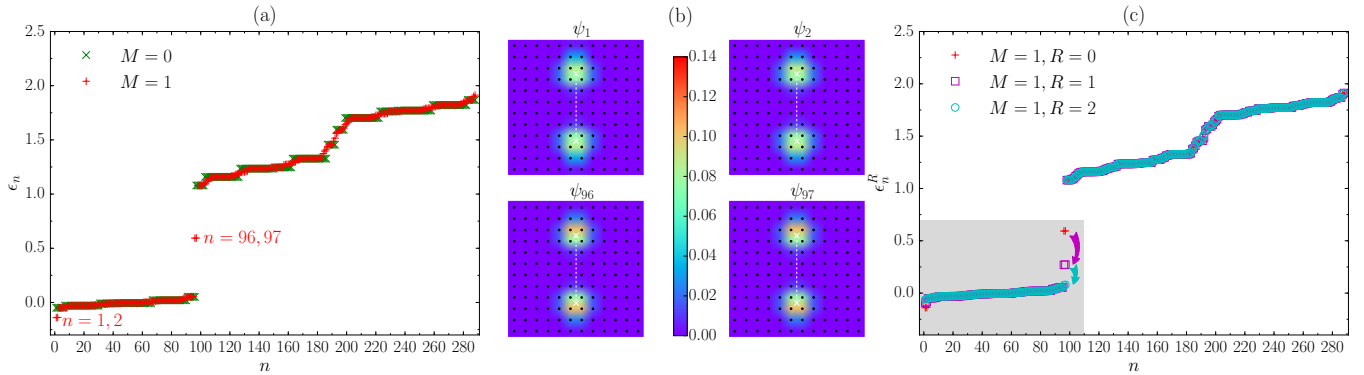


**Figure S2. Single-particle spectra and defect-induced localized states with NN and NNN hopping only.** We show the band structure on a  $L_x \times L_y = 12 \times 12$  lattice with  $\phi = 1/3$ . (a) The single-particle spectrum  $\{\epsilon_n\}$  of  $H'_0$ . In the absence of defects ( $M = 0$ ),  $\epsilon_1, \dots, \epsilon_{96}$  are no longer exactly degenerate at zero energy. With a branch cut ( $M = 1$ , white dashed line) at  $(5.5, 2.5 \rightarrow 8.5)$ , the original band structure is distorted, with two nearly degenerate clusters ( $\epsilon_1, \epsilon_2$ ) and ( $\epsilon_{96}, \epsilon_{97}$ ) having the largest deviation. (b) The lattice site weight of eigenvectors  $\psi_1, \psi_2, \psi_{96}, \psi_{97}$  of  $H'_0$  for the same defects as in (a). All of them are strongly localized near the defects. (c) The single-particle spectrum  $\{\epsilon_n^R\}$  of  $H'_0 + V$  with  $R = 0, 1$ , and  $2$  and the same defects as in (a). The degeneracy of  $\epsilon_1^R, \dots, \epsilon_{97}^R$  (shaded in gray) becomes better for larger  $R$ , with the flatness  $0.7, 2.2, 7.3$  for  $R = 0, 1, 2$ .

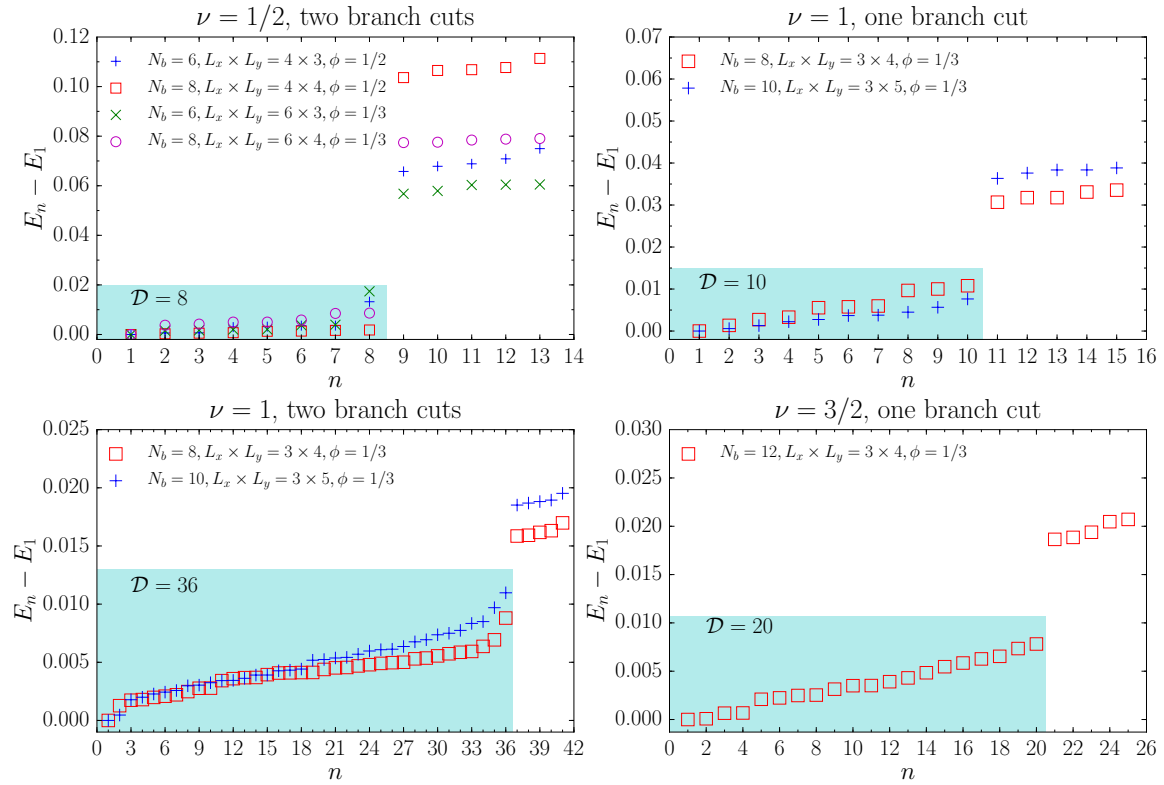


Figure S3. **Defect-enhanced topological degeneracy with NN and NNN hopping only.** We show the many-body spectra resulting from the single-particle Hamiltonian  $H'_0$ . The interactions and branch cut locations in each specific system size are the same as those used in the main text with  $H_0$ . The approximately degenerate ground states, together with the degeneracy  $\mathcal{D}$ , are highlighted by the cyan shade. One can notice that we get the same topological degeneracy as that in the main text.

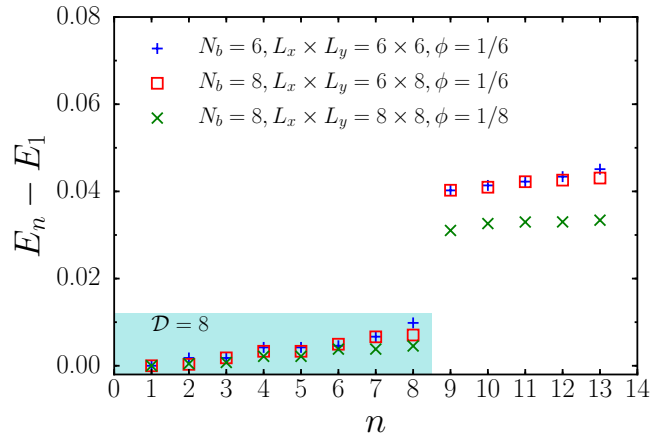


Figure S4. **Defect-enhanced topological degeneracy in the Hofstadter model with defects, for the Abelian  $\nu = 1/2$  state.** We show the many-body calculations with NN hopping only for two branch cuts at  $\nu = 1/2$ . Two branch cuts are located at  $(0.25, 0.5 \rightarrow 3.5), (3.25, 0.5 \rightarrow 3.5)$  for  $L_x \times L_y = 6 \times 6$ ;  $(0.25, 1.5 \rightarrow 5.5), (3.25, 1.5 \rightarrow 5.5)$  for  $L_x \times L_y = 6 \times 8$ ; and  $(1.5, 1.5 \rightarrow 5.5), (5.5, 1.5 \rightarrow 5.5)$  for  $L_x \times L_y = 8 \times 8$ .

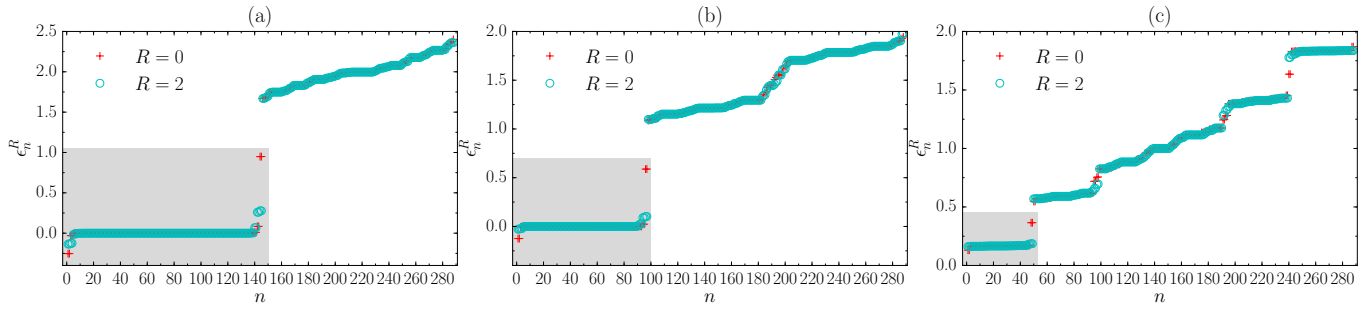


Figure S5. **Flattening the lowest band by a local potential  $\tilde{V}$  including only single-site energies and NN hoppings.** We show the band structure on an  $L_x \times L_y = 12 \times 12$  lattice with a single branch cut ( $M = 1$ ) at  $(5.5, 2.5 \rightarrow 8.5)$ . (a) The single-particle spectrum  $\{\epsilon_n^R\}$  of  $H_0 + \tilde{V}$  at  $\phi = 1/2$  with  $(R, \alpha, \beta) = (0, 0, 0)$  and  $(2, 0.8, -1.4)$ . (b) The single-particle spectrum  $\{\epsilon_n^R\}$  of  $H_0 + \tilde{V}$  at  $\phi = 1/3$  with  $(R, \alpha, \beta) = (0, 0, 0)$  and  $(2, 0.9, -1.3)$ . (c) The single-particle spectrum  $\{\epsilon_n^R\}$  of  $H^{\text{Hof}} + \tilde{V}$  at  $\phi = 1/6$  with  $(R, \alpha, \beta) = (0, 0, 0)$  and  $(2, 1, -1.3)$ , where  $H^{\text{Hof}}$  is the conventional Harper-Hofstadter model with added defects. One can see that, compared to the spectrum without  $\tilde{V}$  correction [ $(R, \alpha, \beta) = (0, 0, 0)$ ], a flat lowest band (shaded in gray) required to stabilize the RR state is indeed established by  $\tilde{V}$ , with a flatness ratio of 3.4, 7.7 and 15.5 in (a), (b) and (c) respectively.

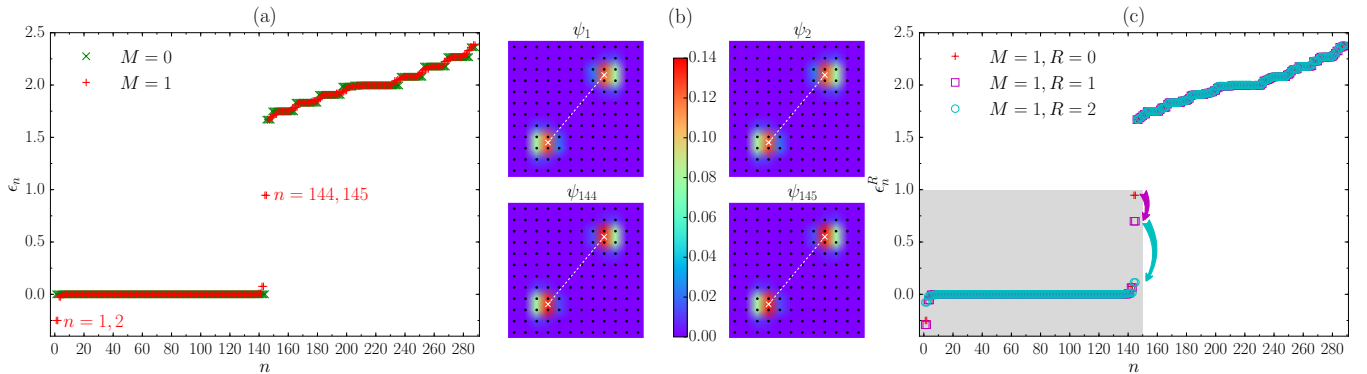
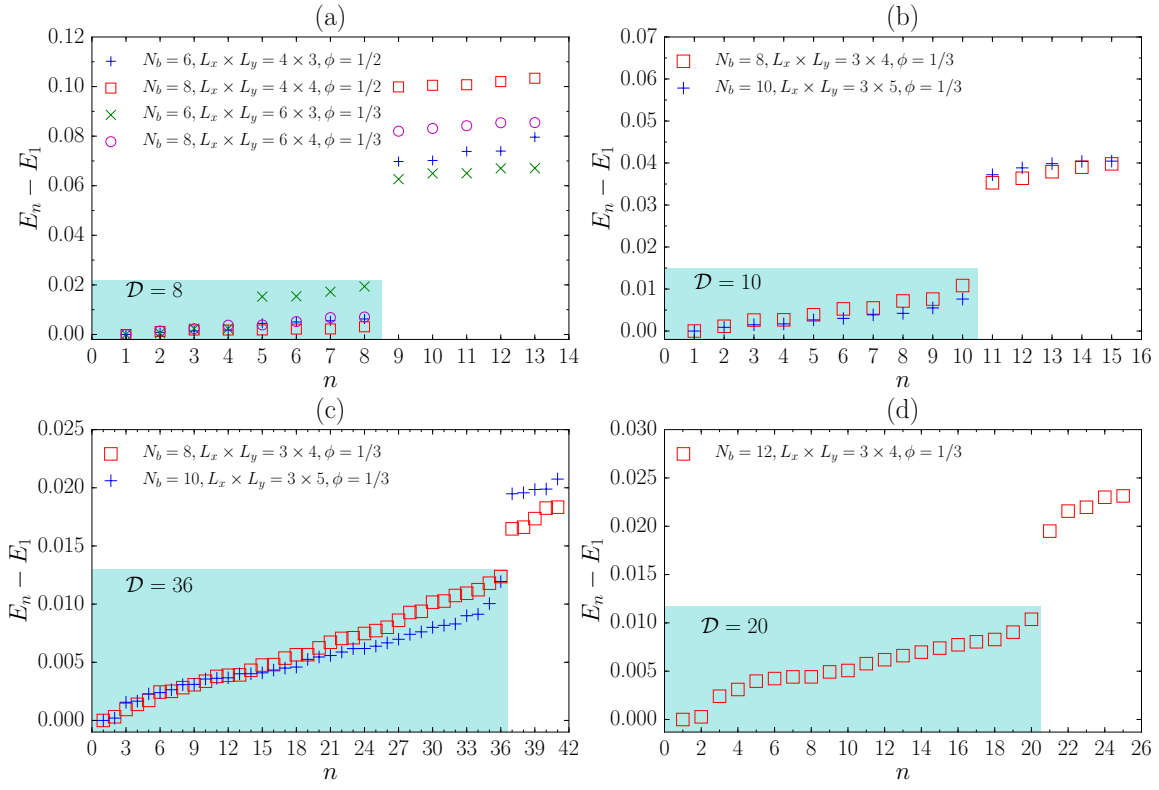


Figure S6. **Single-particle spectra and defect-induced localized states for tilted branch cuts.** We study the band structure on a  $L_x \times L_y = 12 \times 12$  lattice with  $\phi = 1/2$ . (a) The single-particle spectrum  $\{\epsilon_n\}$  of  $H_0$ . In the absence of defects ( $M = 0$ ),  $\epsilon_1, \dots, \epsilon_{144}$  are exactly degenerate at zero energy. With a tilted branch cut ( $M = 1$ , white dashed line) at  $(3, 2.5) \rightarrow (8, 8.5)$ , the original band structure is distorted, with two nearly degenerate clusters ( $\epsilon_1, \epsilon_2$ ) and ( $\epsilon_{144}, \epsilon_{145}$ ) having the largest deviation. (b) The lattice site weight of eigenvectors  $\psi_1, \psi_2, \psi_{144}, \psi_{145}$  of  $H_0$  for the same defects as in (a). All of them are strongly localized near the defects. The eigenstates with less energy deviation from the original band structure, for example,  $\psi_3, \psi_4, \psi_{142}, \psi_{143}$ , are less localized (not shown here). (c) The single-particle spectrum  $\{\epsilon_n^R\}$  of  $H_0 + V$  with  $R = 0, 1$ , and 2 and the same defects as in (a). The degeneracy of  $\epsilon_1^R, \dots, \epsilon_{145}^R$  (shaded in gray) becomes better for larger  $R$ , with the flatness 0.6, 1.0, 8.1 for  $R = 0, 1, 2$ .



**Figure S7. Many-body spectra for tilted branch cuts.** The approximately degenerate ground states, together with the degeneracy  $\mathcal{D}$ , are highlighted by the cyan shade. (a)  $\nu = 1/2$  with two branch cuts at  $(0.25, 0.5) \rightarrow (0.5, 2), (2.25, 0) \rightarrow (2.5, 1.5)$  for  $L_x \times L_y = 4 \times 3$ ;  $(0, 0.75) \rightarrow (1, 2.75), (2, 0.25) \rightarrow (3, 2.25)$  for  $L_x \times L_y = 4 \times 4$ ;  $(0.25, 0.5) \rightarrow (0.5, 2), (3.25, 0) \rightarrow (3.5, 1.5)$  for  $L_x \times L_y = 6 \times 3$ ; and  $(0.5, 0.75) \rightarrow (1.5, 2.75), (3.5, 0.25) \rightarrow (4.5, 2.25)$  for  $L_x \times L_y = 6 \times 4$ . (b)  $\nu = 1$  with one branch cut at  $(0.25, 0.5) \rightarrow (1.75, 2.5)$  for  $L_x \times L_y = 3 \times 4$  and  $(0.25, 0.5) \rightarrow (1.75, 3)$  for  $L_x \times L_y = 3 \times 5$ . (c)  $\nu = 1$  with two branch cuts at  $(0.1, 0.75) \rightarrow (0.4, 2.75), (1.6, 0.25) \rightarrow (1.9, 2.25)$  for  $L_x \times L_y = 3 \times 4$  and  $(0.19, 0.5) \rightarrow (0.31, 3.5), (1.69, 0.45) \rightarrow (1.81, 3.45)$  for  $L_x \times L_y = 3 \times 5$ . (d)  $\nu = 3/2$  with one branch cut at  $(0.5, 0.5) \rightarrow (2, 2.5)$  for  $L_x \times L_y = 3 \times 4$ .